HOKKAIDO UNIVERSITY

Title	Electrochemical performance of a garnet solid electrolyte based lithium metal battery with interface modification
Author(s)	Alexander, George V.; Rosero-Navarro, Nataly Carolina; Miura, Akira et al.
Citation	Journal of Materials Chemistry A, 6(42), 21018-21028 https://doi.org/10.1039/c8ta07652a
Issue Date	2018-11-14
Doc URL	https://hdl.handle.net/2115/76143
Type	journal article
File Information	JMCA Nataly.pdf

Hokkaido University Collection of Scholarly and Academic Papers : HUSCAP

Journal of Materials Chemistry A
View Article Online
DOI: 10.1039/C8TA07652A

Published on 03 October 2018. Downloaded by Hokkaido Daigaku on 10/3/2018 10:32:14 AM.

Journal of Materials Chemistry A Accepted Manuscript

Electrochemical Performance of a Garnet Solid Electrolyte based Lithium Metal Battery with Interface Modification.

George V Alexander [a], Nataly Carolina Rosero-Navarro *[b], Akira Miura[b], Kiyoharu Tadanaga [b], and Ramaswamy Murugan *[a]

a. *High Energy Density Batteries Research Laboratory, Department of Physics, Pondicherry University, Puducherry, 605014, India.*

b. *Division of Applied Chemistry, Faculty of Engineering, Hokkaido University, Sapporo 060-8628, Japan.*

Corresponding authors*:

Email: N.C. Rosero Navarro: rosero@eng.hokudai.ac.jp,

R. Murugan: moranamurugan.phy@pondiuni.edu.in

View Article Online
DOI: 10.1039/C8TA07652A

Published on 03 October 2018. Downloaded by Hokkaido Daigaku on 10/3/2018 10:32:14 AM.

Abstract

Garnet-type $Li_7La_3Zr_2O_{12}$ solid electrolyte is a promising candidate for all-solid-state batteries owing to its high lithium ion conductivity (up to10^{-3} S cm^{-1}) and chemical stability when in contact with lithium metal with a wide electrochemical window of 6V. However, the realization still remains elusive mainly due to the high resistance of electrode/electrolyte interface at room temperature. Although significant improvements have been made toward accomplishing an effective Li metal||garnet solid electrolyte interfaces, the cathode||garnet solid electrolyte interface is challenging due to the rigid morphology of garnet solid electrolyte, poor conductivity and chemical instability of cathode materials. Herein we report an effective strategy of lowering the interfacial resistance between $LiNi_{0.33}Mn_{0.33}Co_{0.33}O_2$ (NMC) and $Li_{6.28}La_3Zr_2Al_{0.24}O_{12}$ (LLZA) solid electrolyte with Li_2SiO_3 (LS) interlayer. The investigation of the NMC||LS-LLZA interface by SEM, adherence test and electrochemical symmetric cell measurement (NMC||LS-LLZA-LS||NMC) revealed that liquid phase derived Li_2SiO_3 buffer layer, not only improves the wettability, but also assists the lithium ion conduction to the active material. On the basis of this improved interface, a bulk type all-solid-state and a *quasi*-solid-state (using Gel Polymer Electrolyte at Li||LLZA interface) lithium metal batteries were fabricated with initial discharge capacities of 138 $mAhg^{-1}$ (100 °C) and 165 $mAhg^{-1}$ (25 °C) at 10 μAcm^{-2} and 100 μAcm^{-2}, respectively. *Quasi*-solid-state battery (NMC||LS-LLZA||GPE||Li) at room temperature displays a capacity retention of 87 % over 50 cycles at higher current density of 100 μAcm^{-2}.

Journal of Materials Chemistry A Accepted Manuscript

View Article Online
DOI: 10.1039/C8TA07652A

Published on 03 October 2018. Downloaded by Hokkaido Daigaku on 10/3/2018 10:32:14 AM.

Journal of Materials Chemistry A Accepted Manuscript

Introduction

Lithium-ion battery (LIB) technology has received significant attention in the last few decades due to its wide application in portable devices, electrical vehicles, and energy storage systems in power plants.[1-3] The highest specific capacity (3860 $mAhg^{-1}$) and lowest electrochemical potential (-3.04 V vs standard hydrogen electrode) of metallic lithium makes it the preferred anode for recharge lithium ion battery.[4] However, owing to safety concerns associated with lithium dendrite formation it has been difficult to achieve a high-energy and power density batteries with the conventional organic liquid electrolytes.[5] Solid state electrolytes with high lithium ion conduction, mechanical and chemical stability against lithium metal have been proposed as a potential candidates for achieving high energy and power density batteries.[6]

Among different solid electrolytes, special attention has been paid to a series of garnet type solid electrolyte because of its striking properties. Among them, zirconia-based garnet electrolyte $Li_7La_3Zr_2O_{12}$ (LLZ) reported by Murugan et al. shows high lithium ion conduction, good chemical stability against lithium metal and substantial electrochemical window.[7-10] Despite these benefits, garnet structured solid electrolytes experience a genuine restriction of making a good interface with electrodes.[11-17] A series of strategies have been reported recently to address the high interfacial resistance between LLZ solid electrolyte and Li metal through metal/metal oxide interlayers. [11-18] Utilization of these functional interlayers enhances the contact amongst LLZ and Li metal by forming a Li-metal alloy which additionally lessens the interfacial obstruction and conquers dendrite growth.[18] However, studies on negating the interfacial resistance between the cathode-LLZ are scanty. Initial reports were centered on forming a thin film of cathode through pulsed laser deposition techniques to accomplish a favorable interface.[19] However, the large scale commercial application of thin-film all-solid-state-battery (ASSB) was restricted by the poor

View Article Online
DOI: 10.1039/C8TA07652A

Published on 03 October 2018. Downloaded by Hokkaido Daigaku on 10/3/2018 10:32:14 AM.

Journal of Materials Chemistry A Accepted Manuscript

electrode mass loadings. Bulk type ASSB's with a large amount of electrode loading are expected to deliver high energy storage capacity, but direct deposition of cathode over LLZ surface fails to form a favorable interface because of poor interfacial contact.[20] High-temperature sintering can enhance the physical contact of cathode over LLZ, but this may lead to the formation of reaction product layer due to elemental cross-diffusion between cathode and LLZ surfaces.[19] Therefore, the critical challenge in achieving a high-performance ASSB lies in the complete separation of cathode and LLZ through high Li^+ conductive, chemically stable and a good bonding buffer layer. A recent report on direct stacking of $LiCoO_2$/NMC-Li_3BO_3 composite cathode over LLZ pellet and simultaneous annealing at 700 °C showed an improvement in the adhesion of composite cathode over LLZ surface.[20-24] However, the improvement in the battery performance was still limited as the addition of the sintering additive to cathode composite and successive sintering of the composite cathode over LLZ pellet didn't ensure an entire separation of cathode with LLZ.[25] As a result, the cathode remained in partial contact with the LLZ, causing a severe reaction between them amid the sintering and charge/discharge process. Hence, it is of upmost importance to develop a strategy for the complete separation of cathode and LLZ via a buffer layer that has high lithium ion conductivity, higher wettability, chemical and electrochemical stability with both cathode and LLZ.[26,27]

In this work, a systematic investigation of $LiNi_{0.33}Mn_{0.33}Co_{0.33}O_2$ (NMC)||$Li_{6.28}La_3Zr_2Al_{0.24}O_{12}$ (LLZA) interface was carried out to reduce the interface resistance. Further, we evaluated the electrochemical performance of Li-metal battery employed with NMC cathode, LLZA solid electrolyte and Li_2SiO_3 as a buffer layer between NMC and LLZA. Li_2SiO_3 could be a strong contender for Li_3BO_3 on account of its reasonable Li+ conductivity and chemical stability.[28] In addition, Li_2SiO_3 which can be easily prepared by liquid-phase process could effectively form a

View Article Online
DOI: 10.1039/C8TA07652A

Published on 03 October 2018. Downloaded by Hokkaido Daigaku on 10/3/2018 10:32:14 AM.

Journal of Materials Chemistry A Accepted Manuscript

thin buffer layer at the NMC||LLZA interface and could improve the cyclability of the battery. Li_2SiO_3 prepared by sol-gel process was expected to improve the wettability since solution containing hydrophilic silanol-species, such as Si-OH, can easily wet the surface of both the garnet pellet and active material particles. A strong covalent linkage was expected to be formed with the oxide surfaces with concomitant loss of organic phases during the curing to remove solvents.[29] It was previously shown that Li_2SiO_3 coating over NMC particle could provide a three-dimensional network of channels beneficial for Li+ migration, which in turn can increase Li+ conduction and thus ameliorate rate capability of NMC particles.[30-32] With the interface treatment, NMC||LLZA interfacial resistance was significantly reduced from 6.5×10^4 Ω cm^2 to 675.3 Ω cm^2 at room temperature (25 °C) and to 351 Ω cm^2 at 100 °C. On the basis of this improved interface, an all-solid-state lithium metal battery and a *quasi*-solid-state battery (using Gel Polymer Electrolyte (GPE) at Li||LLZA interface) based on LLZA as solid electrolyte were fabricated with NMC as cathode and their corresponding battery performance were evaluated. NMC||LS-LLZA||GPE||Li battery at room temperature exhibited an initial discharge capacity of 165 $mAhg^{-1}$ with a capacity retention of 87 % over 50 cycles at a current density of 100 μAcm^{-2}.

Experimental

2.1 Synthesis of $Li_{6.28}La_3Zr_2Al_{0.24}O_{12}$ (LLZA):

High Li^+ conductive cubic phase ($Ia\bar{3}d$) $Li_{6.28}La_3Zr_2Al_{0.24}O_{12}$ (LLZA) lithium garnet was synthesized by solid-state reaction using the following reactants: lithium hydroxide monohydrate ($LiOH.H_2O$, Kanto Chemicals, 98%) (10 wt% excess $LiOH.H_2O$ was added to compensate lithium loss during high temperature sintering), preheated lanthanum oxide (La_2O_3, High Purity Chemicals, 99.9%), aluminum oxide (Al_2O_3, High Purity Chemicals, 99.9%) and zirconium oxide (ZrO_2, Wako). Stoichiometric amount of the reactants were thoroughly ball milled in 2-propanol

View Article Online
DOI: 10.1039/C8TA07652A

Published on 03 October 2018. Downloaded by Hokkaido Daigaku on 10/3/2018 10:32:14 AM.

Journal of Materials Chemistry A Accepted Manuscript

for 12 h. After evaporation of the solvent, the grounded powder was calcined at 950 °C for 12 h in air. The calcined powder was again wet ball milled for 24 h and dried. The dried powder was pressed into pellets and sintered at 1200 °C for 12 h with sufficient amount of mother powder covering the pellets to mitigate lithium loss during sintering. After sintering, LLZA pellets were removed from the mother powder and then polished with 400 and 1200 grit sand paper to control the thickness (~500 µm) and to produce a smooth surface.

2.2 Synthesis of Lithium Silicate:

The Li_2SiO_3 sols were prepared from lithium ethoxide [Li(OEt), High Purity Chemicals, 99.9%] and tetraethoxysilane [TEOS, Shin Etsu, 99%] precursors with an atomic ratio of 2:1 (Li:Si) by sol-gel process.[33] Ethanol was used as a solvent. Stoichiometric amounts of Li(OEt) and TEOS were added to ethanol solution in separate beakers, and were kept for stirring for 2 h. After homogeneous mixing of the precursor solution in ethanol, TEOS solution was added to Li(OEt) under stirring. After 1 h of stirring, hydrolysis was performed by a adding stoichiometric water amount as 0.1 M HCl.

2.3 Preparation of PVdF/PEO polymer blend mat by Electrospin:

PVdF (Sigma Aldrich, M_w= 53,400) and PEO (Sigma Aldrich, M_w= 500,000), were vacuum dried at 60 ºC overnight before use. Solvents, acetone and dimethylformamide (DMF), were used as received. A uniform solution of PVdF (90%) and PEO (10%) in a mixed solvent of acetone/DMF (7:3) was prepared by magnetic stirring for 15 h at room temperature. Polymer/solvent ratio for the final solution were kept at 7 wt. % solid content. A sufficient amount of solution was fed to a 10 mm syringe and the tip of the syringe was connected to a high voltage source. The spun fibers were collected on a grounded, aluminum wrapped plate. Further, the polymer blend mat was dried

View Article Online
DOI: 10.1039/C8TA07652A

at room temperature on the drum followed by vacuum drying at 60 °C for 12 h to remove any trace of solvent.

2.4 Preparation of Composite Cathode:

The pristine NMC [NMC(P)] powder and Li_2SiO_3 sol were dispersed in N-methyl-2-pyrrolidone (NMP) solvent in the mass ratio 70:30 and the total concentration was maintained to be 10 mg ml^{-1}. The particles in the solution were dispersed by ultra-sonication for 2 h and were drop coated onto the surface of Li_2SiO_3 coated LLZA (LS-LLZA). The amount of dropped solution was controlled to achieve ~ 2 $mgcm^{-2}$ active material loading. After dropping, the solvent was evaporated at 300 ºC on a hot plate to achieve composite cathode||LLZA combined structure with an interconnected Li_2SiO_3 buffer layer. After drying, 0.5 $mgcm^{-2}$, acetylene black (AB) dispersed in N-methyl-2-pyrrolidone (NMP) was dropped on the cathode and dried to achieve the current collector.

2.5 Symmetric cells:

LLZA pellets were polished with different grit sized sandpaper to smoothen the surface and also to remove any contamination from the pellet surface. The following symmetric cells were fabricated in a Swagelok type cells to study interface between LLZA and electrode:

(1) NMC(P)||LLZA||NMC(P): The NMC particles were dispersed in NMP solvent with a total concentration maintained to be 10 $mgml^{-1}$. The symmetric cell was fabricated by directly coating pristine NMC particles [NMC(P)] dispersed in NMP solvent over either sides of well-polished LLZA pellet, followed by heat treatment at 300 °C to remove the solvent. Acetylene black dispersed in NMP was dropped and dried on the cathodes to achieve a current collector.

Published on 03 October 2018. Downloaded by Hokkaido Daigaku on 10/3/2018 10:32:14 AM.
Journal of Materials Chemistry A Accepted Manuscript

View Article Online
DOI: 10.1039/C8TA07652A

Published on 03 October 2018. Downloaded by Hokkaido Daigaku on 10/3/2018 10:32:14 AM.

(2) NMC||LLZA||NMC: The symmetric cell was fabricated by coating composite cathode i.e NMC:LS (70:30) [we have denoted composite cathode as NMC] over pristine LLZA pellet followed by heat treatment on either sides in sequence to remove the solvent. Acetylene black dispersed in NMP was dropped and dried on the cathodes to achieve a current collector.

(3) NMC||LS-LLZA-LS||NMC: To prepare the NMC||LS-LLZA-LS||NMC symmetric cell, a thin buffer layer of Li_2SiO_3 was coated above LLZA prior to NMC coating. For coating a thin layer of Li_2SiO_3, a small amount of as-prepared Li_2SiO_3 sol was drop coated on either sides of LLZA and was then heat treated at 300 °C to remove the solvent to form LS-LLZA-LS combined structure. The density of prepared Li_2SiO_3 sol was 3.54 g L^{-1} and the average thickness of Li_2SiO_3 coating over LLZA was estimated to be ~0.5 µm. From the volume and density of Li_2SiO_3, the mass of Li_2SiO_3 coating was calculated to be 35.4 µg. NMC was coated above LS-LLZA-LS structure by a drop casting technique, and the coating was done till the complete surface of LS-LLZA was covered. Later on, NMC||LS-LLZA-LS structure was dried at 300 °C to remove the solvent under air conditions. This was carried out in sequence on either side to form the NMC||LS-LLZA-LS||NMC structure.

(4) Li||GPE|LLZA||GPE||Li: Lithium metal electrodes were punched from lithium belt into round disks and the surface was scratched to remove the oxide coating. The electrospunned PVdf-PEO polymer mat was cut smaller than the size of LLZA pellet. A minimal amount of liquid electrolyte (1.0M $LiPF_6$ in DMC) was poured on to the mat to make it a transparent gel polymer electrolyte (GPE). The symmetric cells were fabricated by placing the GPE between lithium and LLZA pellet.

Journal of Materials Chemistry A Accepted Manuscript

View Article Online
DOI: 10.1039/C8TA07652A

Published on 03 October 2018. Downloaded by Hokkaido Daigaku on 10/3/2018 10:32:14 AM.

Journal of Materials Chemistry A Accepted Manuscript

2.6 Battery Fabrication:

The surface of LLZA pellets were polished and cleaned well before fabricating the battery. The procedure for engineering the surface of LLZA at the cathode side was the same for both all-solid-state battery and *quasi*-solid-state batteries. Initially one side of the LLZA pellet surface was coated with Li_2SiO_3 by drop casting Li_2SiO_3 over LLZA surface, followed by heat treatment at 300 °C to remove the solvent. Later on, composite cathode was drop casted over Li_2SiO_3 coated LLZA surface (LS-LLZA) until the complete surface of LS-LLZA was covered with NMC. Afterwards the solvent was evaporated at 300 ^{o}C to achieve the NMC||LS-LLZA combined structure.

(1) All-solid-state battery: The NMC||LS-LLZA combined structure was utilized for battery fabrication by melting lithium on other side of LLZA pellet with a thin gold (Au) interface to improve the wettability.[18] The cells were assembled in a Swagelok type cell and were heat treated at 180 ^{o}C for 1 hour for the formation of Li-Au alloy to enhance the interfacial contact between lithium and LLZA pellet. The complete fabrication of the all-solid-state battery (NMC||LS-LLZ||Au||Li) was carried out inside an Argon filled glove box.

(2) *Quasi-solid-state* battery: In the case of the *quasi*-solid-state battery, the contact between LLZA and lithium metal was improved by placing a GPE layer in between them. Lithium was punched into a circular disc and the surface was scratched to remove oxide coating. The prepared polymer mat was cut smaller than the size of LLZA pellet to prevent leeching of liquid electrolyte to the cathode side and a controlled amount of liquid electrolyte (5 µL) was poured above the polymer mat to make it as transparent gel and was placed in between LLZA pellet and lithium metal to improve the contact. The Li||GPE||LLZA-LS||NMC cells were assembled in CR2032 coin cell cases inside an Argon filled glove box.

View Article Online
DOI: 10.1039/C8TA07652A

Published on 03 October 2018. Downloaded by Hokkaido Daigaku on 10/3/2018 10:32:14 AM.

Journal of Materials Chemistry A Accepted Manuscript

2.7 Characterization:

Crystal phase analysis of LLZA, composite cathode and LS-LLZA after heat-treatment at 300 ^{o}C were carried out by by XRD (X'pert PRO PANalytical) using a Cu Kα radiation of λ = 1.5418 *Å* in the 2Θ range from 10 to 80°. The Raman spectrum of the garnet surface was measured (Renishaw in via Reflex spectrometer) at room temperature with 50 mW internal Ar^{+} laser source of excitation wavelength 514 nm. The density of the pellet was determined from the physical dimension and weight of the sample using the Archimedes principle. The morphologies of the interfaces and surface were investigated using a scanning electron microscope (Miniscope® TM3030Plus, Hitachi).

2.7.1 Electrochemical Measurements:

The Electrochemical Impedance Spectroscopic (EIS) measurements, galvanostatic cycling with potential limitation tests and cyclic voltammetry were carried out with Bio-Logic VMP 3, SI 1260 Solartron and 580 battery type system, Scribner Associates. The two sides of LLZA pellet were sputtered with Au to form a blocking electrode for the ionic conductivity measurement. EIS measurements were carried out over the frequency range of 1 MHz to 1 Hz at a perturbation amplitude of 10 mV. Constant current cycling of the Li||GPE||LLZA||GPE||Li symmetric cell was conducted with a current density of 0.4 mA cm $^{-2}$, over a period of ~ 0.2 h. For the all-solid-state battery, the temperature was controlled at 100 ºC by placing the batteries in a temperature chamber and the cell was cycled with a constant current of 10 μAcm^{-2} in the voltage range of 2-4.5 V. For *quasi*-solid-state battery, the cell was cycled with different current density of 50 μAcm^{-2} and 100 μAcm^{-2} in the voltage range of 2.0 - 4.5 V at room temperature (25 °C). To check the stability of

View Article Online
DOI: 10.1039/C8TA07652A

Published on 03 October 2018. Downloaded by Hokkaido Daigaku on 10/3/2018 10:32:14 AM.

Journal of Materials Chemistry A Accepted Manuscript

composite cathode, a CV scan was performed in a voltage range of 2.0 V – 4.6 V at a scan rate of 0.1 mV s^{-1}.

3. Results and Discussion

3.1 Characterization of LLZA

A high lithium ion conductive and dense solid electrolyte is crucial for the high performance of an all-solid-state battery. The powder X-ray diffraction (XRD) pattern and Raman spectrum of $Li_{6.28}La_3Zr_2Al_{0.24}O_{12}$ (LLZA) pellet along with the reported pattern of high Li^+ conductive high temperature cubic phase LLZ are displayed in Figure 1a and 1b, respectively, The powder X-ray diffraction and Raman spectrum of the synthesized LLZA samples confirm the high Li^+ conductive cubic phase of lithium garnet ($Ia\bar{3}d$). Earlier Raman studies on lithium garnets suggested that the Raman bands observed between 100 and 150 cm^{-1} corresponds to La cation, the broad and fairly overlapping Raman band observed between 200 and 500 cm^{-1} corresponds to the internal modes of LiO_6 and LiO_4 and is due to the dynamic disorder of highly mobile lithium ion.[34-36]

The impedance data was fitted with the equivalent circuit shown as inset in Figure 1c. From the fitting result the semicircle at high-frequency regime seems to be mainly related to bulk response and the grain boundary contribution appears to be negligible. The total (grain + grain boundary) Li^+ conductivity of LLZA was calculated to be 3×10^{-4} S cm^{-1} (Figure 1c) at 25 °C. The density of LLZA pellet quantitatively evaluated by Archimedes method was found to be around 94%. The cross-sectional SEM image of LLZA as shown in Figure 1d is predominantly trans granular and the grain boundary is difficult to distinguish, indicating a tight connection between the grains.

3.2 Characterization of NMC//LS-LLZA-LS//NMC symmetric cell

View Article Online
DOI: 10.1039/C8TA07652A

Published on 03 October 2018. Downloaded by Hokkaido Daigaku on 10/3/2018 10:32:14 AM.

Journal of Materials Chemistry A Accepted Manuscript

The XRD patterns of pristine NMC, Li_2SiO_3 and composite NMC cathode have been portrayed in Figure S1. The XRD pattern of pristine NMC was well determined as α-$NaFeO_2$ structure with the space group R3/m. The XRD pattern of Li_2SiO_3 shows a broad pattern because of its amorphous nature. However, for the composite cathode (NMC:LS) the intensity of initial peak at 2Θ = 19° was suppressed compared to pristine NMC cathode because of the presence of amorphous Li_2SiO_3. Moreover, no peak shift or secondary phases were observed in the composite cathode, indicating that the coating of Li_2SiO_3 remains in the composite as amorphous phase and does not influence the original structure of layered material.

The XRD pattern of LS-LLZA obtained after heat treatment at 300 °C is presented in Figure S2. For the XRD pattern of Li_2SiO_3 coated LLZA sample, a suppressed peak at 2Θ = 16.86 ° was observed compared to the XRD pattern of pristine LLZA. However, it was further noted that all other peaks were in match with the peaks of LLZA. The depressed peak at 16.86 ° could be because of thin layer of amorphous Li_2SiO_3. It was noticed that no peak shift and no impurity peaks were observed confirming the stability of Li_2SiO_3 coated over LLZA. Additional information regarding the phase composition and structure of LS-LLZA was obtained using Raman spectroscopy and the recorded Raman spectra of LS-LLZA and bare LLZA are both shown in Figure S3. The Raman modes of the collected spectrum (LS-LLZA) matches well with the reported Raman spectrum of cubic garnet phase[34] which confirms that LS-LLZA after heat treatment at 300 °C have the single phase of cubic garnet structures.

The effect of Li_2SiO_3 as a buffer layer between NMC and LLZA was qualitatively assessed by simple peel-off experiment (adherence test) and from cross-sectional SEM images. For the peel-off experiment, adhesive tape was stuck with NMC and then peeled from the surface of NMC coated over pristine LLZA and LS-LLZA. It was observed that for pellets without Li_2SiO_3 coating

View Article Online
DOI: 10.1039/C8TA07652A

Published on 03 October 2018. Downloaded by Hokkaido Daigaku on 10/3/2018 10:32:14 AM.

Journal of Materials Chemistry A Accepted Manuscript

on LLZA surface, NMC was easily detached after the peel-off experiment because of poor wetting ability of NMC with LLZA pellet. From the cross-sectional SEM image in Figure 2a, interfacial gaps were observed between LLZA and NMC resulting in poor interfacial contact. In contrast, NMC remains well-adhered to LS-LLZA surface in equivalent peel-off experiments because of firm contact between NMC and LS-LLZA. From the cross-sectional SEM observation (as shown in Figure 2b), it is evident that the Li_2SiO_3 interfacial layer over LLZA surface is in micron size range with an average thickness of 0.5 μm. The homogenous thin Li_2SiO_3 buffer layer helps to form good bonding between NMC and LLZA. The elemental mapping images as shown in Figure 2c-e, were taken based on Figure 2b. The corresponding La, Si and Co elemental map shows distinct layers of LLZA, LS and NMC, respectively.

To quantify the effect of Li_2SiO_3 as buffer layer for improving NMC||LLZA interface contact, symmetric cells were fabricated and tested with EIS. Figure 3a shows the Cole-Cole plot of NMC(P)||LLZA||NMC(P). From the equivalent circuit, the charge transfer resistance between NMC and LLZA was estimated as 6.5×10^4 Ω cm^2. The high charge transfer resistance is an evidence of poor interfacial contact. The impedance spectrum of NMC||LLZA||NMC demonstrates an interfacial resistance of ~ 7200 Ω cm^2 for each side as shown in Figure 3b. This reduction in interfacial resistance can be ascribed to improved wettability of the composite cathode with LLZA surface. Although the composite cathode was able to reduce the interfacial resistance, the reduction of resistance at the interface was limited as an effective contact area between LLZA and cathode was poor.

The EIS plot of NMC||LS-LLZA-LS||NMC symmetric cell in Figure 3c describes the interfacial resistance between NMC and LLZA with Li_2SiO_3 buffer layer. The impedance curve was fitted with the equivalent circuit shown as inset in Figure 3c. From the fitting data the curve contains a

View Article Online
DOI: 10.1039/C8TA07652A

Published on 03 October 2018. Downloaded by Hokkaido Daigaku on 10/3/2018 10:32:14 AM.

Journal of Materials Chemistry A Accepted Manuscript

grain and grain boundary resistance at the higher frequency regime, charge transfer resistance between LLZA and NMC at the middle frequency and the diffusion impedance at the lower frequency regime. The charge transfer resistance of NMC||LS-LLZA-LS||NMC is approximately 675.3 Ω cm^2 for each side which originates from LS||LLZA and LS||NMC interface. The corresponding fitting results are shown in Figure S4. The decrease in interfacial resistance can be attributed to the following reasons: (i) the addition of Li_2SiO_3 fills the voids in LLZA and creates a homogeneous and better contact between LLZA and NMC and (ii) thin layer of Li_2SiO_3 coating assists the lithium conduction to the active material and provides a good adherence to the solid electrolyte thus reducing the interfacial resistance. In order to elucidate the impedance contribution of the LS-LLZA interface, EIS of a symmetric cell with LS-LLZA-LS configuration was conducted as shown in Figure S5. The impedance spectrum was fitted with an equivalent circuit shown as inset in Figure S5. From the fitting result, LS-LLZA impedance contribution was measured to be 23 Ω cm^2. In addition, it has been observed that when the operating temperature was raised to 100 °C, the interfacial resistance of NMC||LS-LLZA-LS||NMC was reduced from 675.3 Ω cm^2 to 351 Ω cm^2 as shown in Figure 3d. The symmetric cell showed a distinct semicircle with a significant decrease in the interfacial resistance and the cathode diffusion impedance indicating that a higher operating temperature can effectively improve the NMC||LS-LLZA contact and reduce the interfacial resistance. A summary on the effect of Li_2SiO_3 buffer layer on the interfacial resistance on the cathode side is given in Figure 3e. We envision that with further optimization on the thickness of Li_2SiO_3 layer by spin coating or dip coating technique, it is possible to reduce the interfacial resistance even further.

3.3 Electrochemical Characterization of Batteries

View Article Online
DOI: 10.1039/C8TA07652A

Published on 03 October 2018. Downloaded by Hokkaido Daigaku on 10/3/2018 10:32:14 AM.

Journal of Materials Chemistry A Accepted Manuscript

Li metal batteries based on LLZA pellet were fabricated with a Li_2SiO_3 buffer layer on the cathode side and the corresponding battery performance was evaluated.

3.3.1 Electrochemical Performance of all-solid-state battery

The electrochemical characterization of the fabricated all-solid-state battery is shown in Figure 4. Figure 4a shows a schematic of Li-metal battery design using Li_2SiO_3 buffer layer. The interfacial resistance between lithium metal and garnet was estimated using a Li||Au||LLZA||Au||Li symmetric cell. From the impedance curve in Figure S6, the aerial interfacial resistance was calculated to be ~1900 Ω cm^2 (for each side) at 25 °C. Figure 4b shows the EIS plot of NMC||LS-LLZA||Au||Li full cell, tested at different temperatures (25 °C and 100 °C). The impedance curve was fitted with an equivalent circuit as shown in Figure S7. From the fitting data the curve contains a grain and grain boundary resistance at higher frequency regime, charge transfer resistance between LLZA pellet and electrode at middle frequency and the diffusion impedance at lower frequency regime. It was observed that the bulk resistance, interfacial resistance and the diffusion impedance all decrease significantly as the operating temperature increases. The interfacial resistance decreased from 3700 Ω cm^2 at 25 °C to ~800 Ω cm^2 at 100 °C, respectively. The decrease in resistance can be attributed to the improved conductivity of LLZA pellet and the well-formed favorable interface at higher temperature. A NMC||LLZA||Li battery was fabricated without any interface modification for comparison. Figure S8 shows the electrochemical performance of NMC||LLZA||Li cell at 100 °C. The cell delivered a poor initial discharge capacity of 46 $mAhg^{-1}$ owing to the lack of physical contact. The fabricated NMC||LLZA||Li battery was unable to cycle with good performance at room temperature because of low diffusivity of lithium ions through the interface. On the other hand, the NMC cathode in the all-solid-state battery (NMC||LS-LLZA||Au||Li) with interface modification delivered an initial discharge capacity of 138 $mAhg^{-1}$

View Article Online
DOI: 10.1039/C8TA07652A

Published on 03 October 2018. Downloaded by Hokkaido Daigaku on 10/3/2018 10:32:14 AM.

Journal of Materials Chemistry A Accepted Manuscript

when cycled in a voltage range from 4.5 to 2 V (Figure 4c). It should be noted that a low cut-off voltage for the discharge process has been used to allow a suitable lithium intercalation in the battery. The kinetics of the lithium intercalation is expected to be reduced because of relatively low ionic conductivity of the lithium silicate buffer layer (compared with Li-ion batteries) and therefore slowing down the charge transfer in the solid-solid interfaces. The NMC||LS-LLZA||Au||Li battery shows cycling stability for 10 cycles with a coulombic efficiency of almost 100 % (Figure 4d). The improved interface between NMC and LLZA pellet was helpful to enhance the cell performance but with further cycling we observed capacity fading which can be ascribed to the high polarization of the cell. However, more detailed in-situ investigations and a post mortem analysis of the fabricated batteries are necessary for further understanding the reasons for capacity fading.

3.3.2 Electrochemical Performance of quasi-solid-state battery.

For application at room temperature (25°C), a *quasi*-solid-state battery was fabricated. On the lithium side, a gel interlayer was used at the interface as the gel layer could provide a soft and continuous contact between LLZA and Li metal. Figure 5a shows the SEM image of the prepared polymer blend mat. The mat consisted of fine fibers that could provide adequate mechanical strength for handling. The inset shows the photograph of the polymer mat. A minimal amount of liquid electrolyte was poured on the mat to make a transparent gel polymer electrolyte. To identify the interfacial resistance between metallic lithium and LLZA, Li||GPE||LLZA||GPE||Li symmetric cells were tested by electrochemical impedance spectroscopy at room temperature. The impedance profile of Li||GPE||LLZA||GPE||Li symmetric cell contains the bulk and grain boundary resistance in the high frequency region, and the interfacial resistance in the low frequency region (Figure S9a). From the Cole-Cole plot, the interfacial areal specific resistance was calculated to be 332 Ω

View Article Online
DOI: 10.1039/C8TA07652A

Published on 03 October 2018. Downloaded by Hokkaido Daigaku on 10/3/2018 10:32:14 AM.

Journal of Materials Chemistry A Accepted Manuscript

cm^2 for each side at room temperature. Galvanostatic cycling studies were performed on Li||GPE||LLZA||GPE||Li symmetric cell to mimic the operation of charging and discharging of lithium metal batteries. From Figure S9b, the Li||GPE||LLZA||GPE||Li symmetric cell cycled for 25 h shows stable cycling at 0.4 $mAcm^{-2}$ with small overpotential, indicating a significant reduction in interfacial resistance compared to Li||LLZA without any interface modification (Figure S9c). The inset in Figure S9b shows that the resistance was constant during each cycle of Li stripping/plating. During galvanostatic cycling, the total interfacial resistance calculated from Ohms law was 750 Ω cm^2, that when divided by two is 325 Ω cm^2 for each of the two Li||GPE||LLZA interface, which was in good agreement with the results obtained from impedance spectroscopy. The observed constant resistance during lithium stripping/platting cycling is possibly due to stable interface, small interfacial resistance and homogeneous contact provided by the gel interlayer.

To further test the performance of Li_2SiO_3 and GPE in a full cell configuration, a *quasi*-solid-state battery with NMC||LS-LLZA||GPE||Li architecture was assembled as shown in Figure 5b. The impedance curve of NMC||LS-LLZA||GPE||Li at room temperature exhibits overall resistance of 1187 Ω cm^2, which was close to the sum of NMC||LS-LLZA interface and LLZA||GPE||Li interface as depicted in Figure 5c. The impedance data was fitted with an equivalent circuit shown as inset in Figure 5c. The CV scan of NMC||LS-LLZA||GPE||Li was done at a scan rate of 0.1 mVs^{-1} in the potential window of 2.0 V – 4.6 V. Interestingly, the oxidation/reduction peaks of Co^{3+}/Co^{4+} couple lying in between 4.4V~5V [37] was found stable with cycles. The broad peaks of 3.47 V for positive scan and 3.31 V for negative scan corresponds to Ni^{2+}/Ni^{4+} couples. The two peaks of nickel couples were separated by 0.16 V indicating that the total resistance across the cell is high when compared to that of conventional battery. All the peaks were found stable for several

View Article Online
DOI: 10.1039/C8TA07652A

Published on 03 October 2018. Downloaded by Hokkaido Daigaku on 10/3/2018 10:32:14 AM.

cycles (1 to 4) as shown in Figure 5d. The charge-discharge cycling of the cell was performed at different current densities of 50 μAcm^{-2} and 100 μAcm^{-2} respectively. The cell delivered an initial discharge capacity of 165 mAhg^{-1} in the voltage range of 4.5-2.0 V at 100 μA cm^{-2} as shown in Figure 5d. Even after applying high current density, the battery displayed a capacity of 144 mAhg^{-1} after 50 cycles, which indicated that the NMC||LS-LLZ interface remains stable. Figure 5e portrays the discharge capacity and columbic efficiency of NMC||LS-LLZA||GPE||Li quasi solid-state battery cell at different current densities of 50 μA cm^{-2} and 100 μA cm^{-2} over 75 cycles. The coulombic efficiency greater than 97% during cycling indicates the good electrochemical stability of LS-LLZA against NMC.

4. Conclusion

In summary, we have demonstrated an effective strategy to address the high resistance at NMC||LLZA interface. The liquid phase process of Li_2SiO_3 buffer layer could easily wet the surface of both NMC and LLZA resulting in the reduction of interfacial resistance from 6.5×10^4 Ω cm^2 to 675.3 Ω cm^2 (25 °C) and 351 Ω cm^2 (100 °C). An all-solid-state battery consisting of NMC cathode, LLZA pellet and Li-metal anode demonstrated an initial discharge capacity of 138 mAh g^{-1} and stable cycling performance over 10 cycles at 100 °C. In addition, a *quasi*-solid-state battery at room temperature with an initial discharge capacity of 165 mAhg^{-1} shows stable cycling over 50 cycles at higher current density of 100 μAcm^{-2}. The present investigation shows that micron sized Li_2SiO_3 layer not only wets both NMC and LLZA pellet but also assists the lithium conduction to the active material and provides good adherence to the solid electrolyte. Therefore, it is critical to consider choose the proper interfacial layer material and design of the interfacial structure between the electrodes and solid electrolyte for the improved performance of ASS lithium metal batteries.

Journal of Materials Chemistry A Accepted Manuscript

View Article Online
DOI: 10.1039/C8TA07652A

Published on 03 October 2018. Downloaded by Hokkaido Daigaku on 10/3/2018 10:32:14 AM.

Journal of Materials Chemistry A Accepted Manuscript

Conflicts of interest

There are no conflicts of interest to declare.

Acknowledgement

The present study was partially supported by KAKENHI Grant 17K17559, Japan. G.V.A. thanks the Advanced Graduate School of Chemistry and Materials Science (AGS) of Hokkaido University who has supported his short-term stay. R.M. acknowledges SERB-DST, New Delhi India for their support (EMR/2017/000417).

View Article Online
DOI: 10.1039/C8TA07652A

Published on 03 October 2018. Downloaded by Hokkaido Daigaku on 10/3/2018 10:32:14 AM.

Journal of Materials Chemistry A Accepted Manuscript

References

[1] J. B. Goodenough, and Y. Kim, *Chem. Mater*, 2009, ***22*(3)**, 587-603.

[2] M. Armand and J. M. Tarascon, *Nature*, 2008, **451**, 652-657.

[3] Y. Kato, S. Hori, T. Saito, K. Suzuki, M. Hirayama, A. Mitsui, M. Yonemura, H. Iba, and R. Kanno, *Nature Energy*, 2016, ***1*(4)**, 16030.

[4] G. Girishkumar, B. McCloskey, A. C. Luntz, S. Swanson, and W. Wilcke , *J. Phys. Chem. Lett.*, 2010, **1**, 2193−2203.

[5] W. Xu, J. Wang, F. Ding, X. Chen, E. Nasybulin, Y. Zhang, J.-G. Zhang, *Energy Environ. Sci.*, 2014, **7**, 513–537.

[6] J. E. Trevey, J. R. Gilsdorf, C. R. Stoldt, S. H. Lee, and P. Liu, *J. Electrochem. Soc.*, 2012, **159**, A1019−A1022.

[7] R. Murugan, V. Thangadurai and W. Weppner, *Angew. Chem. Int. Ed*., 2007**, 46**, 7778-7781.

[8] W. Xia, B. Xu, H. Duan, Y. Guo, H. Kang, H. Li and H. Liu, *ACS Appl. Mater. Interfaces*, 2016, **8**, 5335-5342.

[9] W.D. Richards, L.J Miara, Y. Wang, J.C Kim and G. Ceder, *Chem. Mater.*, 2016, **28**, 266-273.

[10] C. Deviannapoorani, L. Dhivya, S. Ramakumar, and R. Murugan. *J. Power Sources*, 2013, **240**, 18-25.

[11] K.K. Fu, Y. Gong , B. Liu ,Y. Zhu , S. Xu , Y. Yao , W. Luo , C. Wang , S.D Lacey , J. Dai, Y. Chen ,Y. Mo, E.D Wachsman and L.Hu, *Sci. Adv*., 2017, **3**, 1601659.

[12] W. Luo, Y. Gong, Y. Zhu, Y. Li, Y. Yao, Y. Zhang, K.K. Fu, G. Pastel, C.F. Lin, Y. Mo and E.D. Wachsman. *Adv. Mater.*, 2017, **29**, 1606042 (1-7)

[13] W. Luo, Y. Gong, Y. Zhu ,K.K. Fu, J. Dai , S.D. Lacey ,C. Wang , B. Liu , X. Han, Y. Mo, E.D. Wachsman, *J. Am. Chem. Soc*., 2016, **138**, 12258-12262.

View Article Online
DOI: 10.1039/C8TA07652A

Published on 03 October 2018. Downloaded by Hokkaido Daigaku on 10/3/2018 10:32:14 AM.

[14] X. Han , Y. Gong , K.K Fu , X. He ,G.T Hitz , J. Dai , A. Pearse , B. Liu ,H. Wang, G. Rubloff , Y. Mo, V. Thangadurai, E.D. Wachsman, L. Hu , *Nature Materials*, 2017, **16**, 572-579.

[15] C.L. Tsai , V. Roddatis , C.V. Chandran , Q. Ma , S. Uhlenbruck , M. Bram., P. Heitjans , and O. Guillon, *ACS Appl. Mater. Interfaces.*, 2016, **8**, 10617-26

[16] C. Wang, Y. Gong, B. Liu, K. Fu, Y. Yao, E. Hitz, Y. Li, J. Dai, S. Xu, W. Luo, E.D. Wachsman, *Nano lett*., 2016, **17**, 565-571.

[17] A. Sharafi, Y. Seungho, N. Michael, M. Lee, M. Cheng, H. M. Meyer, J. Nanda, M.Chi, D. J. Siegel, and J. Sakamoto, *J. Mater. Chem. A.*, 2017, **5(26)**, 13475-13487.

[18] G. V. Alexander, S. Patra, S.V.S Raj, M. K. Sugumar, M. M. U. Din, and R. Murugan, *J. Power Sources*, 2018, *396*, 764-773.

[19] K. H. Kim, Y. Iriyama, K. Yamamoto, S. Kumazaki, T. Asaka, A. Tanabe, C. A. Fisher, T. Hirayama, R. Murugan and Z. Ogumi, *J. Power Sources*, 2011, ***196*(2)**, 764-767.

[20] T. Kato, T. Hamanaka, K. Yamamoto, T.Hirayama , F. Sagane, M. Motoyama, and Y. Iriyama, *J. Power Sources*, 2014, **260**, 292-298.

[20] K. Park, B.C. Yu , J.W. Jung, Y. Li , W. Zhou, H. Gao, S. Son, J.B. Goodenough. *Chem. Mater*., 2016, **28**, 8051-8059.

[21] S. Ohta, S. Komagata, J. Seki , T. Saeki, S. Morishita, T. Asaoka, *J. Power Sources*, 2013, **238**, 53-56.

[22] M. Shoji, H. Munakata, K. Kanamura, *Front. Energy Res*., 2016, **4**, 32

[23] T. Liu, Y. Ren, Y. Shen, S. X. Zhao, Y. Lin, and C. W. Nan, *J. Power Sources*, 2016, **324**, 349-357.

[24] T. Liu, Y. Zhang, X. Zhang, L. Wang, S. X. Zhao, Y.H. Lin, Y. Shen, J. Luo, L. Li, and C. W. Nan, 2018. *J. Mater. Chemi. A*, 2018, **6**, 4649-4657.

Journal of Materials Chemistry A Accepted Manuscript

View Article Online
DOI: 10.1039/C8TA07652A

Published on 03 October 2018. Downloaded by Hokkaido Daigaku on 10/3/2018 10:32:14 AM.

[25] K. Park, B. C. Yu,, J. W. Jung,, Y. Li, W. Zhou, H. Gao, S. Son, and J. B. Goodenough, *Chem. Mater.*, 2016, ***28*(21)**, 8051-8059.

[26] A. Sakuda, H. Kitaura, A. Hayash, K. Tadanaga, and M. Tatsumisago, *J.Power Sources*, 2009, ***189*(1)**, 527-530.

[27] K. Takada, N. Ohta, L. Zhang, K. Fukuda, I. Sakaguchi, R. Ma, M. Osada, and T. Sasaki, *Solid State Ionics*, 2008, **179(27-32)**, 1333-1337.

[28] S.I. Furusawa, T. Kasahara, and A. Kamiyama, *Solid State Ionics*, 2009, ***180*(6-8)**, 649-653.

[29] Arkles B. Hydrophobicity, hydrophilicity and silanes: Water, water everywhere is the refrain from the rhyme of the ancient mariner and a concern of every modern coatings technologist. *Paint Coat. Ind.* **2006** Oct.

[30]S.I. Furusawa, T. Kasahara, and A. Kamiyama, *Solid State Ionics*, 2009, **180(6-8)**, 649-653.

[31] G. Hu, M. Zhang, L. Wu, Z. Peng, K. Du, and Y. Cao, *J. Alloy Compd*, 2017, **690**, 589-597.

[32] G. Yang, G. Jia, X. Shangguan, Z. Zhu, Z. Peng, Q. Zhuge, F. Li, and X. Cui, 2017. *J. Electrochem Soc.*, 2017, **164(12)**, A2889-A2897.

[33] A. Sakuda, H. Kitaura, A. Hayashi, K. Tadanaga, and M. Tatsumisago, *Electrochem. Solid State Lett.*, 2008, ***11*(1)**, A1-A3.

[34] L. Dhivya, R. Murugan, *ACS Appl. Mater. Interfaces*, 2014, **6**, 17606-17615.

[35] G. Larraz, A. Orera, M.L. Sanjuan, *J. Mater. Chem. A, 2013*, **1**, *11419-11428.*

[36] C.M. Julien, M. Massot, *Mater. Sci. Eng.,B* ,2003, **100**, *69-78.*

[37] X. Zhang, C. Zhenlian, S. Björn, S. Florian, E. Helmut, K. An, Z. Zhang, Q. Zhang, Y. Li, and J. Li, *Electrochim. Acta*, 2017, **227**, *152-161*.

Journal of Materials Chemistry A Accepted Manuscript

View Article Online
DOI: 10.1039/C8TA07652A

Published on 03 October 2018. Downloaded by Hokkaido Daigaku on 10/3/2018 10:32:14 AM.

Journal of Materials Chemistry A Accepted Manuscript

Figure and Caption:

Caption:

Figure 1**:** (a) XRD pattern of LLZA disk (red) and reported high temperature cubic LLZ (black) [7]. (b) Raman spectrum of LLZA (red) sintered at 1200 °C measured in the range of 50 to 1000 cm^{-1} along with the reported high temperature cubic LLZ (black). (c) Nyquist plot of LLZA with blocking electrodes on both side measured at room temperature (25 °C). The impedance data was fitted with the equivalent circuit where R_1 corresponds to total resistance and Q_1 corresponds to constant phase element of LLZA. (d) Zoomed in cross-sectional SEM image of LLZA pellet.

Figure 2: (a) Digital image of the peel-off experiment and cross-sectional SEM image of NMC||LLZA||NMC. Interfacial voids are seen between NMC and LLZA because of poor wettability of LLZA and NMC (b) Digital image of the peel-off experiment and the cross-sectional SEM image of NMC||LS-LLZA-LS||NMC. NMC was firmly attached to the LLZA pellet after peel off experiment because of firm contact. A micron size Li_2SiO_3 buffer layer is observed between NMC and LLZA. Elemental mapping on the cross-section of NMC||LS-LLZA-LS||NMC with distinct layers of (c) La, (d) Si and (e) Co.

Figure 3: (a) Cole-Cole plot of NMC(P)||LLZA||NMC(P) symmetric cell, measured at 25 °C. The impedance data was fitted with the equivalent circuit shown as inset in which R_1 corresponds to bulk resistance, R_2 corresponds to grain boundary impedance and Q_2 corresponds to constant phase element of LLZA, R_3 and Q_3 corresponds to charge transfer resistance and double layer capacitance on NMC||LLZA interface, W_4 and Q_4 corresponds to diffusion impedance inside of the cathode. (b) Cole-Cole plot of NMC||LLZA||NMC symmetric cell measured at 25 °C. The impedance data was fitted with the equivalent circuit shown as inset (c) Cole-Cole plot of

View Article Online
DOI: 10.1039/C8TA07652A

Published on 03 October 2018. Downloaded by Hokkaido Daigaku on 10/3/2018 10:32:14 AM.

Journal of Materials Chemistry A Accepted Manuscript

NMC||LS-LLZA-LS||NMC symmetric cell measured at 25 °C. The inset shows the corresponding equivalent circuit in which R_1 corresponds to bulk resistance, R_2 grain boundary impedance and Q_2 corresponds to constant phase element of LLZA, R_3 and Q_3 corresponds to charge transfer resistance and double layer capacitance on NMC||LS interface, R_4 and Q_4 corresponds to charge transfer resistance and double layer capacitance on LS||LLZA interface and W_5 and Q_5 corresponds to diffusion impedance inside of cathode. (d) Cole-Cole plot of NMC||LS-LLZA-LS||NMC symmetric cell measured at 100 °C. The inset shows the corresponding equivalent circuit in which R_1 corresponds to bulk resistance, R_2 grain boundary impedance and Q_2 corresponds to constant phase element of LLZA, R_3 and Q_3 corresponds to charge transfer resistance and double layer capacitance on NMC||LS interface, R_4 and Q_4 corresponds to charge transfer resistance and double layer capacitance on LS||LLZA interface and W_5 and Q_5 corresponds to diffusion impedance inside of cathode (e) Schematic comparison of LLZA||NMC interfacial resistance with and without Li_2SiO_3 buffer layer.

Figure 4 (a) Schematic of all-solid-state battery with Li_2SiO_3 buffer layer at NMC side and a metallic Au interlayer at lithium side. (b) Cole-Cole plot of NMC||LS-LLZA||Au||Li full cell, tested under different temperatures (25 °C and 100 °C) along with the fitting results. (c) Charge-discharge profile of NMC||LS-LLZA||Au||Li full cell, cycled from 4.5V to 2V at 100 °C. (d) Discharge capacity and Coulombic efficiency of NMC||LS-LLZA||Au||Li full cell cycled at 10 μAcm^{-2} for 10 cycles.

Figure 5: (a) SEM image of the prepared polymer mat. The inset shows the digital image of polymer mat.(b) Schematic of the fabricated *quasi*-solid-state battery cell, with Li_2SiO_3 buffer layer on the cathode side, and GPE on the anode side. (c) Cole-Cole plot of NMC||LS-LLZA||GPE||Li *quasi* solid-state battery cell tested at 25 °C. The impedance data was fitted with

View Article Online
DOI: 10.1039/C8TA07652A

the equivalent circuit shown as inset in which R_1 corresponds to bulk resistance, R_2 corresponds to grain boundary impedance and Q_2 corresponds to constant phase element of LLZA, R_3 and Q_3 corresponds to charge transfer resistance and constant phase element of LS||LLZA and GPE||LLZA interface, R_4 and Q_4 corresponds to charge transfer resistance and constant phase element of LS||NMC and GPE||Li interface and W_5 and Q_5 corresponds to diffusion impedance inside of cathode. (d) CV of NMC||LS-LLZA||GPE||Li cell, measured at a scan rate of 0.1 mVs^{-1}. (e) Charge- Discharge profile of NMC||LS-LLZA||GPE||Li *quasi* solid-state battery cell cycled at 100 μAcm^{-2} for 50 cycles. (f) Discharge capacity and coulombic efficiency of *quasi* solid-state battery cell cycled at 50μAcm^{-2} and 100 μAcm^{-2} over 75 cycles with good capacity retention.

Published on 03 October 2018. Downloaded by Hokkaido Daigaku on 10/3/2018 10:32:14 AM.

Journal of Materials Chemistry A Accepted Manuscript

View Article Online
DOI: 10.1039/C8TA07652A

Published on 03 October 2018. Downloaded by Hokkaido Daigaku on 10/3/2018 10:32:14 AM.

Figures:

Figure 1:

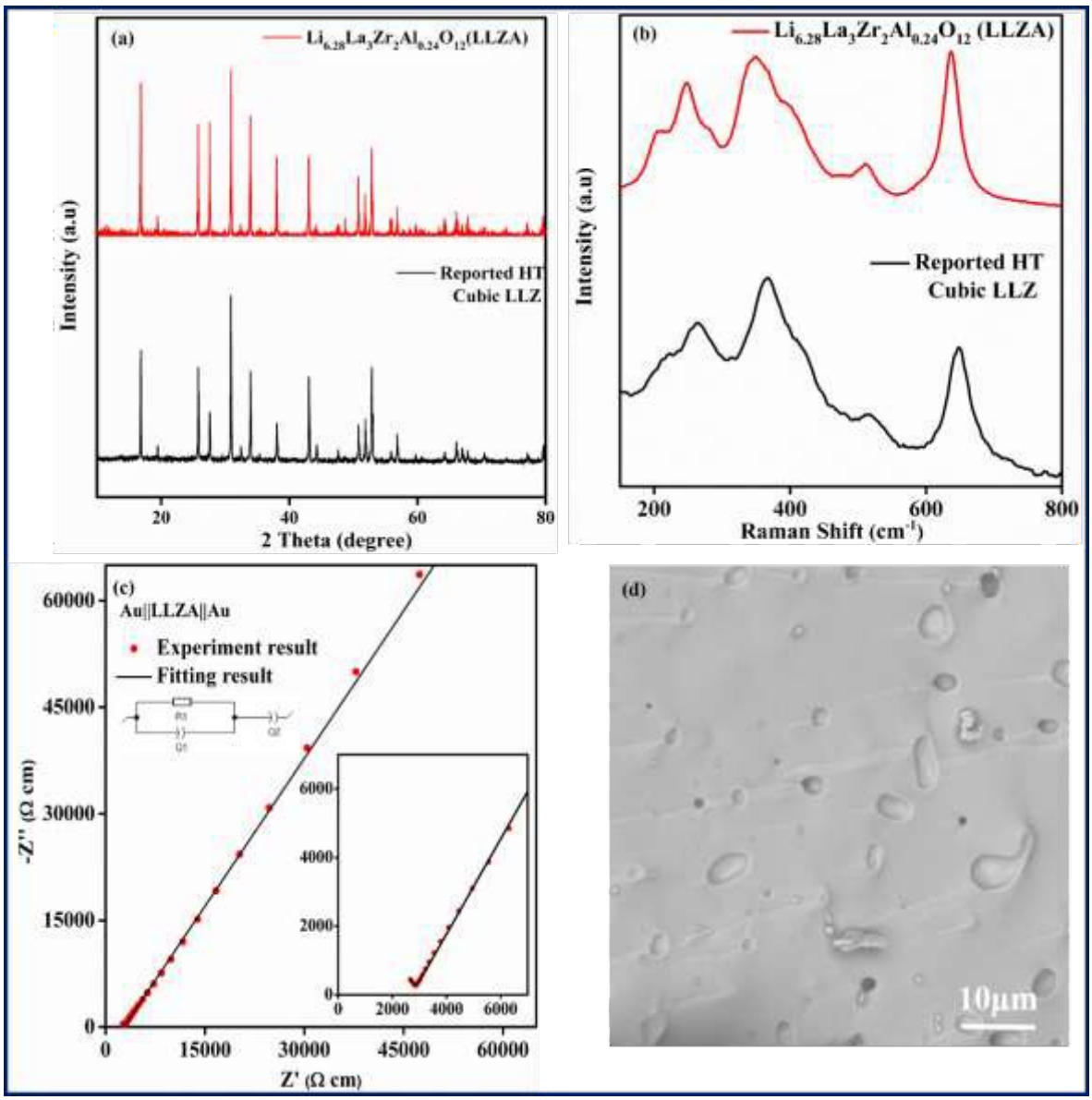

Journal of Materials Chemistry A Accepted Manuscript

View Article Online
DOI: 10.1039/C8TA07652A

Published on 03 October 2018. Downloaded by Hokkaido Daigaku on 10/3/2018 10:32:14 AM.

Figure 2:

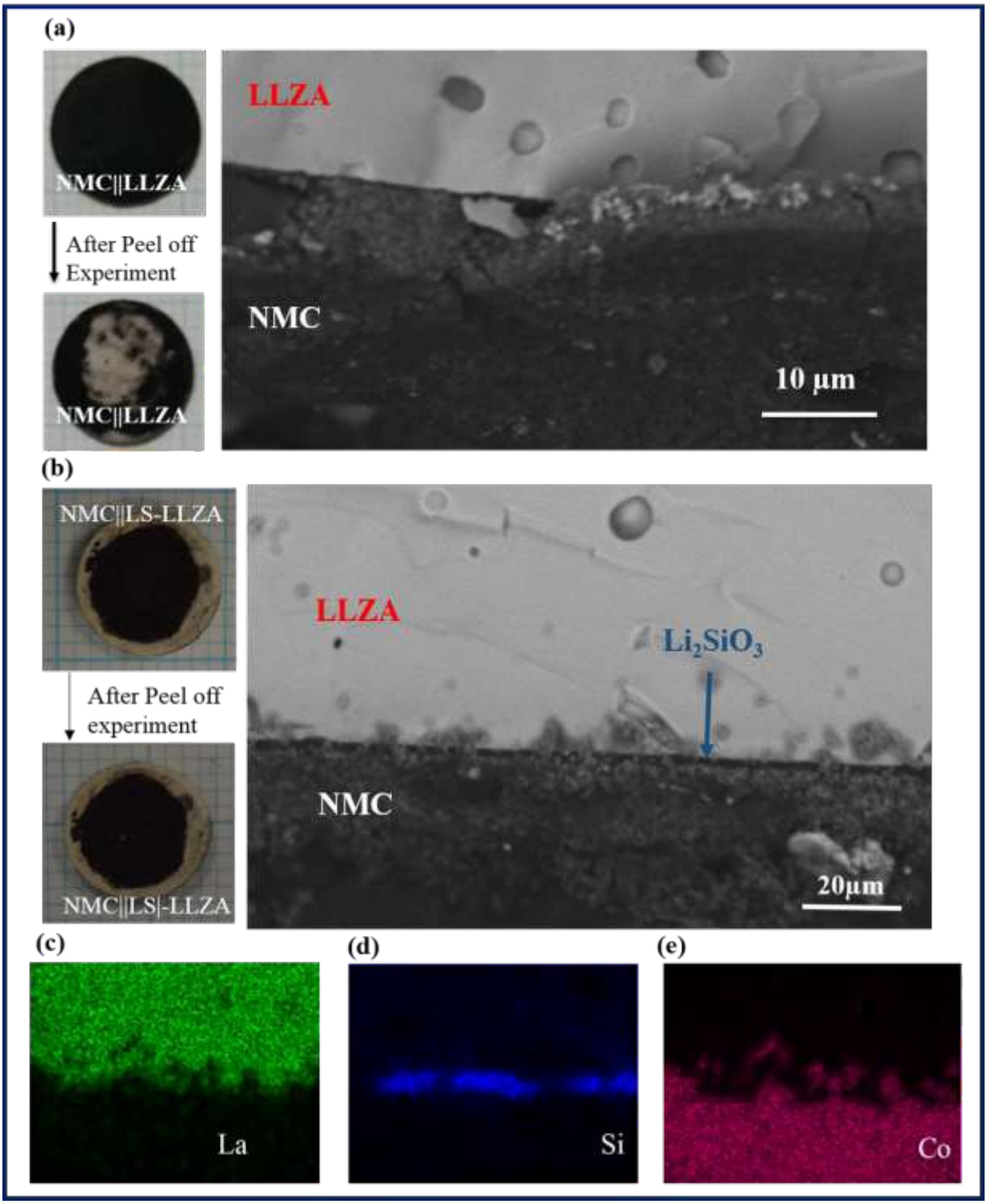

Journal of Materials Chemistry A Accepted Manuscript

View Article Online
DOI: 10.1039/C8TA07652A

Published on 03 October 2018. Downloaded by Hokkaido Daigaku on 10/3/2018 10:32:14 AM.

Figure 3:

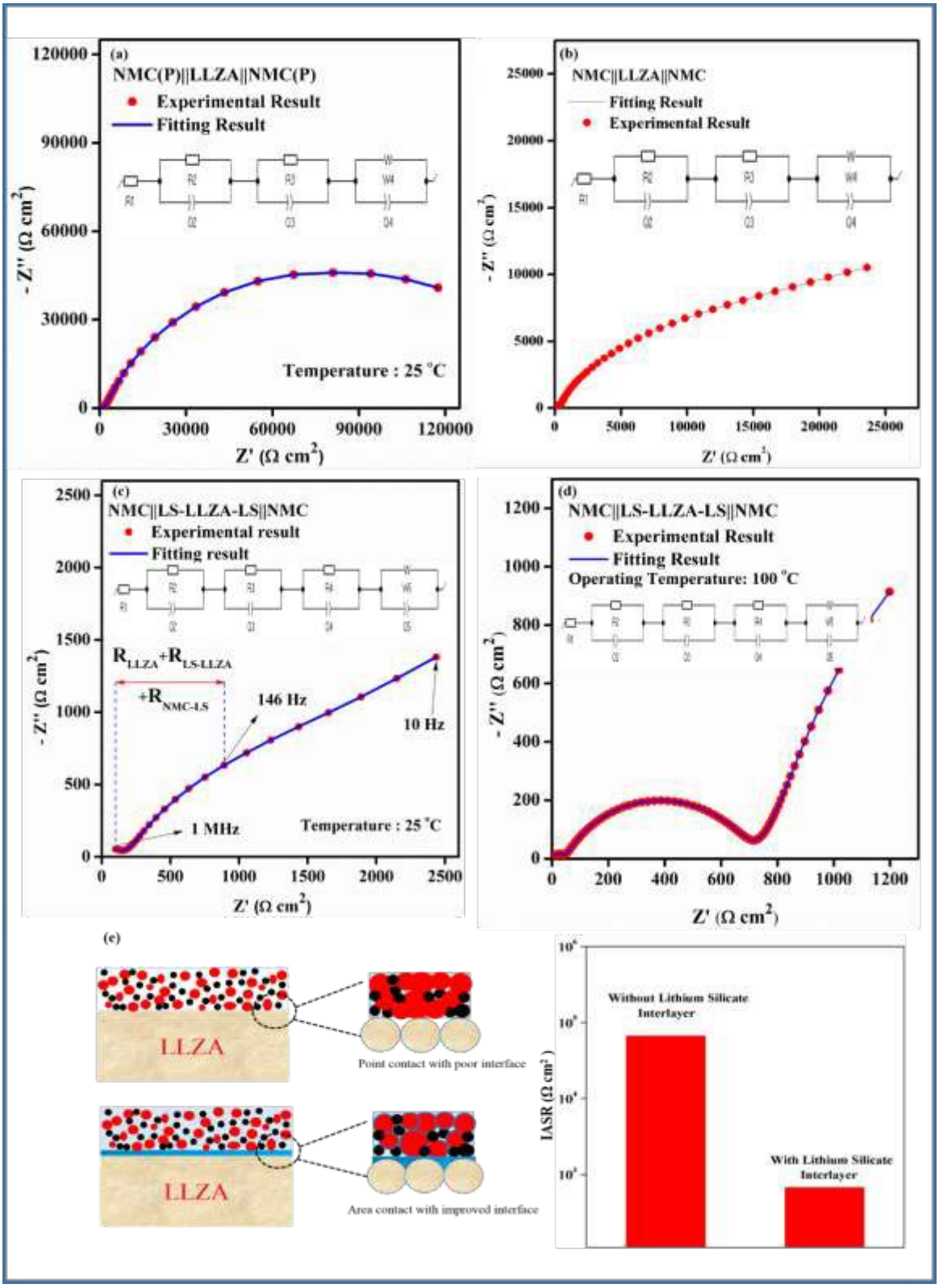

Journal of Materials Chemistry A Accepted Manuscript

View Article Online
DOI: 10.1039/C8TA07652A

Published on 03 October 2018. Downloaded by Hokkaido Daigaku on 10/3/2018 10:32:14 AM.

Figure 4:

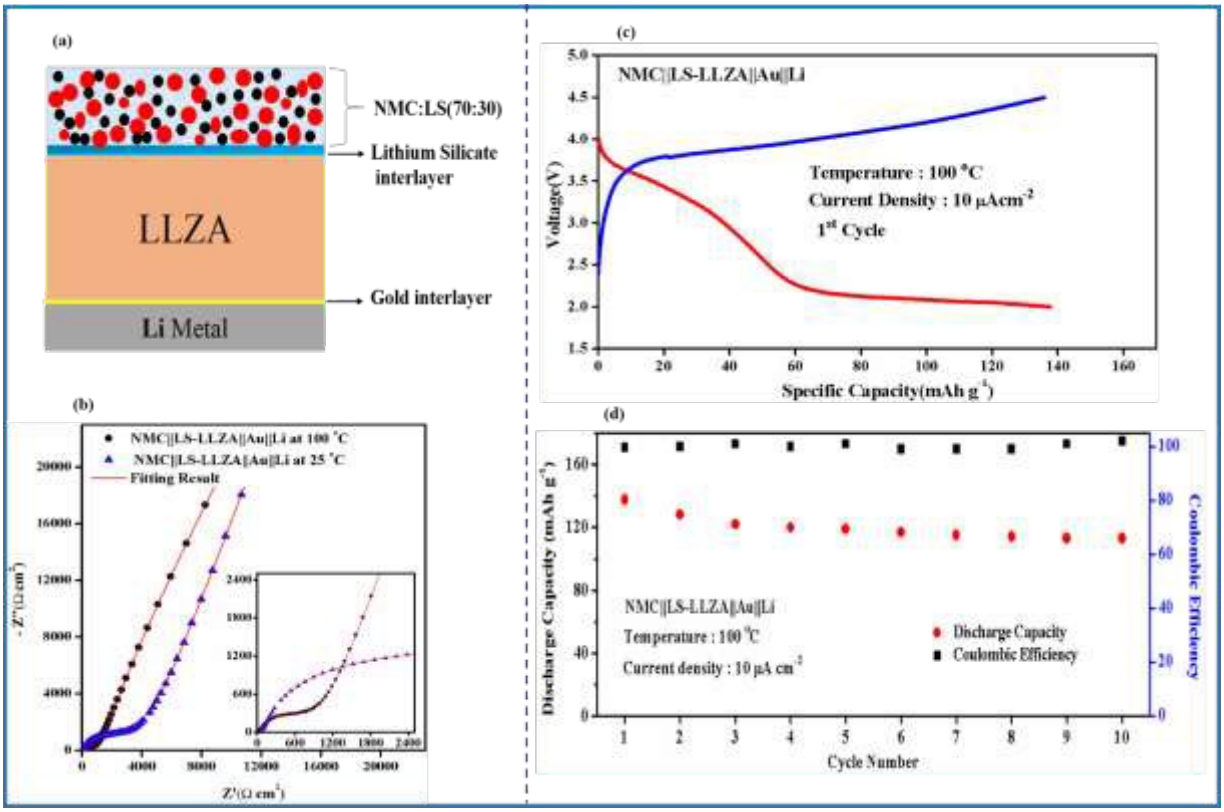

Journal of Materials Chemistry A Accepted Manuscript

View Article Online
DOI: 10.1039/C8TA07652A

Published on 03 October 2018. Downloaded by Hokkaido Daigaku on 10/3/2018 10:32:14 AM.

Figure 5:

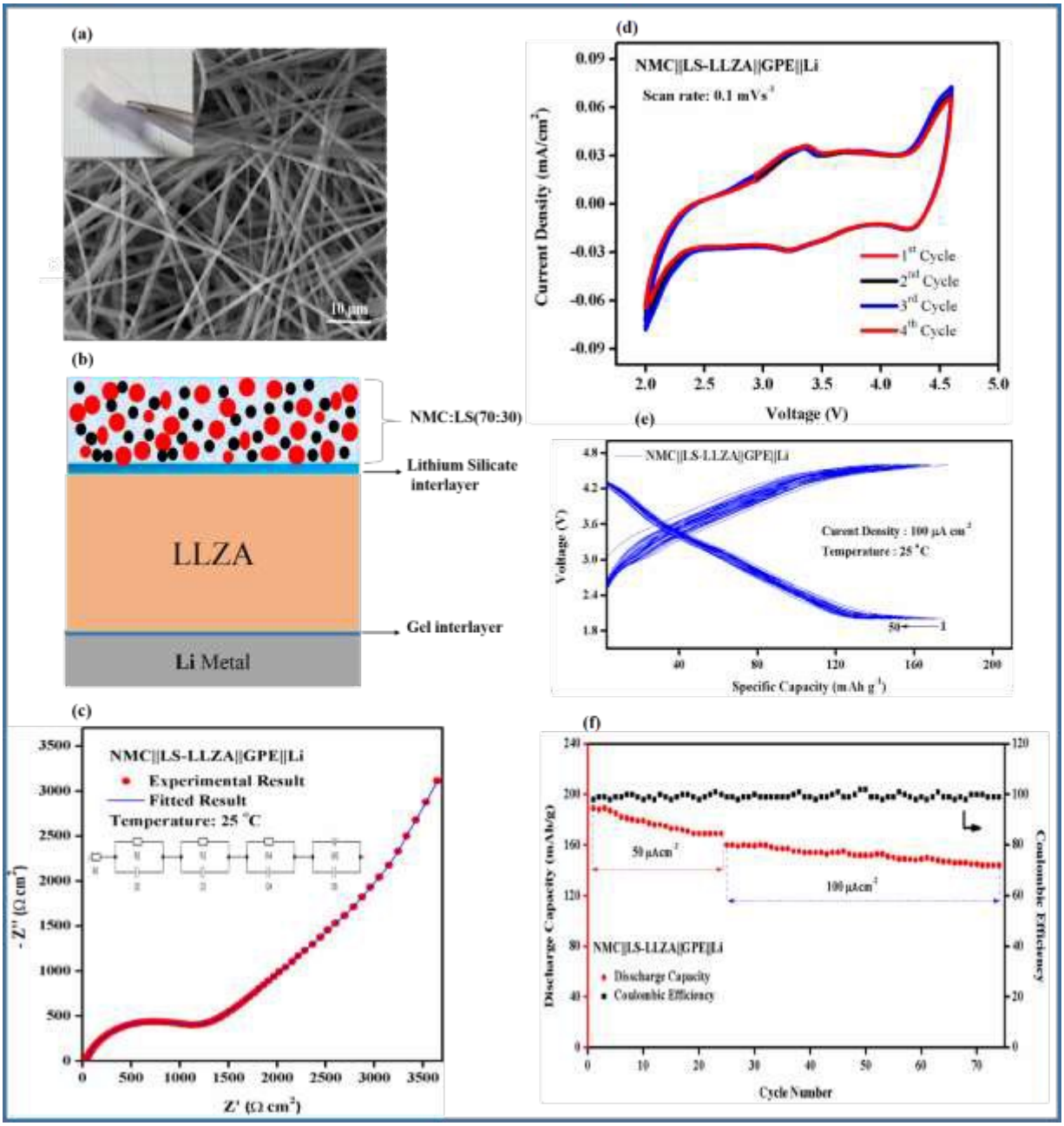

Journal of Materials Chemistry A Accepted Manuscript

View Article Online
DOI: 10.1039/C8TA07652A

Published on 03 October 2018. Downloaded by Hokkaido Daigaku on 10/3/2018 10:32:14 AM.

Graphical Abstarct:

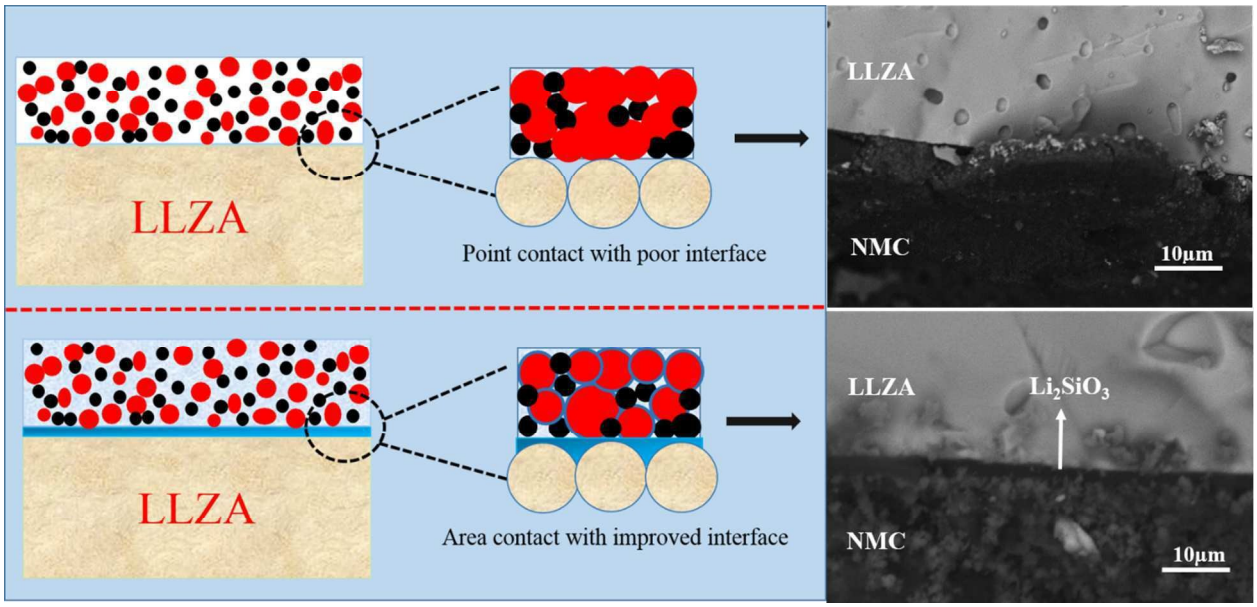

An effective strategy to lower interfacial resistance between NMC and garnet-structured solid electrolyte with Li_2SiO_3 interlayer

Journal of Materials Chemistry A Accepted Manuscript